Electrical Power and Energy Systems 123 (2020) 106243

Contents lists available at ScienceDirect

Electrical Power and Energy Systems

journal homepage: www.elsevier.com/locate/ijepes

Enhanced harmonic state estimation in unbalanced three-phase electrical grids based on the Kalman filter and physical scale-down implementation

Ismael Molina-Moreno[a], Aurelio Medina[b,*], Rafael Cisneros-Magaña[b], Olimpo Anaya-Lara[c], Juan Alfonso Salazar-Torres[a]

[a] División de Estudios de Posgrado e Investigación, Instituto Tecnológico de Morelia, Tecnológico Nacional de México, Morelia 58120, Mexico
[b] Facultad de Ingeniería Eléctrica, División de Estudios de Posgrado, U.M.S.N.H., Ciudad Universitaria, C.P. 58030 Morelia, Michoacán, Mexico
[c] Institute for Energy and Environment, Department of Electronic and Electrical Engineering, University of Strathclyde, Glasgow, UK

ARTICLE INFO

Keywords:
Harmonic state estimation
Numerical Differentiation
Kalman filter
Practical data
Unbalanced condition

ABSTRACT

A time-domain methodology is proposed based on Kalman filter, to determine the harmonic state estimation in three-phase electrical grids. Time-domain methodologies based on the Kalman filter need an initial solution to begin estimating the harmonic state in electrical grids. Previous methods have found this solution using simulated electrical grids; thus, the measurements taken from the simulations are synchronised only with the simulated grid model. In practical power networks, measurements taken from the grid need to be synchronised with the theoretical grid model. Synchronization between the model and measurements using the Kalman filter is proposed. This paper also proposes an alternative method to obtain the periodic steady-state solution in power grids. The method adequately processes the information given by a limited number of measurements to find the required solution. An experimental case study for a three-phase unbalanced condition with a nonlinear load and a limited number of measurements is used to validate the proposed methodology, i.e. practical data has been used instead of synthetic data. Hence, the results are validated by direct comparison of the state estimation response against the actual data recorded from the experimental laboratory implementation. The results show that using the proposed methodology, the time-domain harmonic state estimation can be efficiently applied to the analysis of practical power grids.

1. Introduction

Power quality (PQ) is an important concern in the operation of power systems due to many reasons, but the ultimate reason is the economic [1]. PQ problems encompass a wide range of different phenomena such as electromagnetic transients, voltage fluctuations, and harmonic distortion, among others. A detailed description of adverse PQ events is reported in [1–3]. As interconnected power systems can be of large scale, global PQ assessment has practical limitations due to the restricted number of monitoring points and insufficient knowledge of the system parameters; hence, power quality state estimation (PQSE) has been addressed [4–7]. Harmonic state estimation (HSE) [8–16], which is one of the issues covered by PQSE, will be analysed in this research work.

In HSE analysis, harmonics can be represented in the frequency domain [8–10] as well as in the time-domain [11–17]. It is more convenient to represent the harmonic spectrum by its harmonic components, i.e. by the amplitude and the phase of each harmonic component [8–10]. Time-domain simulators such as the electromagnetic transient with direct current program (EMTDC®) [18,19] or Simulink® are used to analyse the response to specific harmonic sources through distorted signal waveforms. The potential of the time-domain approach is that the measurement process is less complex than the one used in the frequency domain. Further, it obtains and processes the information regarding harmonics. The registered distorted waveforms implicitly contain an infinite number of harmonic components.

Reference [11] proposes a time-domain HSE (TDHSE) methodology to estimate the harmonic state in power systems, based on the Kalman filter (KF). Since the power grid is modelled by a set of first-order ordinary differential equations (ODE), an initial state is required. The simulation starts from zero as initial condition and the periodic steady-state solution is obtained by Poincare map and extrapolation to the limit cycle, using the numerical differentiation (ND) procedure [20,21]. However, this solution needs to be synchronised with the

* Corresponding author.
E-mail addresses: imolina@itmorelia.edu.mx (I. Molina-Moreno), amedinr@gmail.com (A. Medina), rcisneros@dep.fie.umich.mx (R. Cisneros-Magaña), olimpo.anaya-lara@strath.ac.uk (O. Anaya-Lara).

https://doi.org/10.1016/j.ijepes.2020.106243
Received 4 April 2020; Received in revised form 3 May 2020; Accepted 1 June 2020

measurements when they are taken from the physical electrical grid.

Reference [12] proposes a method that exploits the half-wave symmetry in the voltage and current waveforms to make the ND method more efficient in obtaining the periodic steady-state solution for the KF algorithm. Again, as the measurements are taken from the simulation, i.e. they are not synchronized with the physical electrical grid.

Reference [13] proposes a method based on KF as in [11,12] where the measurements are taken from a scale-down test system set up, i.e. using experimental data instead of synthetic data. However, the method has been evaluated only for a balanced condition. In addition, as the test power system is experimental, the measurements can be capacitor voltages and inductor currents. In a practical power grid, sending and receiving end line currents must be the available measurements for transmission lines.

References [14–16] propose a method to evaluate the TDHSE, where an accurate initial state is not needed. The method considers the grid parameters to be exact. However, the uncertainty of the parameters should be considered.

This research work proposes a time-domain methodology to estimate the harmonic state, where measurements are taken from the physical electrical grid. The proposed methodology is performed in three steps: first, by using a limited number of measurements taken from the electrical grid, an algorithm based on the KF to obtain a fast periodic steady-state solution is proposed; second, by exploiting the half-wave symmetry, the current and voltage waveforms are obtained using half-cycle; and third, by applying the fast Fourier transform (FFT) to evaluate the harmonic content in a waveform signal, the frequency domain harmonic state is obtained.

The remaining paper is organised as follows: Section 2 describes the proposed methodology; Section 3 details the experimental low-order model of the electrical grid to validate the proposed methodology; Section 4 reports and compares the results obtained with the proposed methodology against those obtained from the laboratory test system response and Section 5 draws the main conclusions from this research work.

2. Proposed methodology

The complete scheme for the TDHSE problem is shown in Fig. 1. The description of the blocks is detailed next.

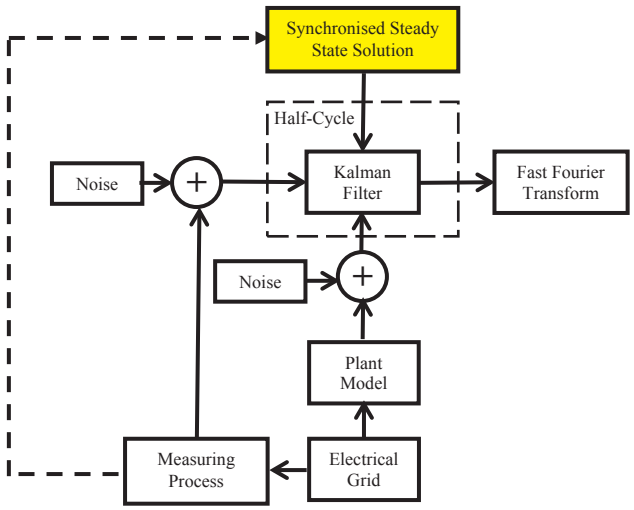

Fig. 1. Complete scheme of the time-domain harmonic state estimation problem.

2.1. Plant modelling

The power system can be modelled in the state-space framework through a first-order ordinary differential equation (ODE) set, i.e.

$$d\mathbf{x}/dt = \mathbf{A}\mathbf{x}(t) + \mathbf{B}\mathbf{u}(t) \tag{1}$$

where $\mathbf{x} \in \mathbb{R}^N$ is the state vector, $\mathbf{A} \in \mathbb{R}^{N\times M}$ is the state matrix, $\mathbf{u} \in \mathbb{R}^R$ is the input vector, and $\mathbf{B} \in \mathbb{R}^{N\times R}$ is the input matrix. Matrices $\mathbf{A}$ and $\mathbf{B}$ are formed by the parameters of the electrical grid components such as transmission lines, capacitive banks, transformers and synchronous generators.

The observable outputs are usually defined by

$$\mathbf{y}(t) = \mathbf{C}\mathbf{x}(t) + \mathbf{D}\mathbf{u}(t) \tag{2}$$

where $\mathbf{y} \in \mathbb{R}^{\boldsymbol{M}}$ is the output vector, namely the observable outputs, i.e. the outputs that can be measured such as busbar voltages and sending or receiving line currents. $\mathbf{C} \in \mathbb{R}^{\boldsymbol{M\times N}}$ is the output matrix that defines which variables are measured and $\mathbf{D} \in \mathbb{R}^{\boldsymbol{N\times N}}$ is the direct transmission matrix that is usually assumed as zero. A detailed procedure to build the matrices $\mathbf{A}$, $\mathbf{B}$, $\mathbf{C}$, and $\mathbf{D}$ of the plant model in (1–2) is reported in [11].

The continuous time-domain plant model formulated by (1–2) can be transformed into a discrete time formulation through several methods [22] if $\boldsymbol{t}$ is discretised as,

$$t[k] = kT_S \tag{3}$$

where T_S is the sample period, and k is the *k-th* sample. The discrete transformation of (1–2) results in,

$$\mathbf{x}[k+1] = \mathbf{\Phi}\mathbf{x}[k] + \mathbf{G}\mathbf{u}[k] \tag{4}$$

$$\mathbf{z}[k] = \mathbf{H}\mathbf{x}[k] \tag{5}$$

where the notation of kT_S is represented by k, $\mathbf{\Phi} \in \mathbb{R}^{N\times N}$ is the transition state matrix, $\mathbf{G} \in \mathbb{R}^{N\times R}$ is the discrete input matrix, $\mathbf{H} \in \mathbb{R}^{M\times N}$ is the measurement matrix, and $\mathbf{z} \in \mathbb{R}^M$ is the output measurement vector taken from the electrical grid, having the system M measurements and N states.

The Nyquist theorem states that the minimum sampling frequency $F_S = 1/T_S$ must be,

$$F_S = 2fh \tag{6}$$

where f is the fundamental frequency and h is the maximum harmonic order.

2.2. Kalman filter algorithm

The plant modelled by (4–5) does not consider the errors in the plant model parameters and measurements. In order to consider the uncertainty of the parameters in the plant model given by (4), as well as the error in the measurements given by (5), the complete plant model used by the KF algorithm is redefined as,

$$\mathbf{x}[k+1] = \mathbf{\Phi}\mathbf{x}[k] + \mathbf{G}\mathbf{u}[k] + \mathbf{w}[k] \tag{7}$$

$$\mathbf{z}[k] = \mathbf{H}\mathbf{x}[k] + \mathbf{v}[k] \tag{8}$$

where $\mathbf{w} \in \mathbb{R}^N$ and $\mathbf{v} \in \mathbb{R}^M$ are the error vectors associated to the plant model and measurements model, respectively. These errors can be modelled as random noise.

The KF algorithm and its variants [23–26] are based on minimising the squared error $\mathbf{e} \in \mathbb{R}^{\boldsymbol{N}}$, defined as,

$$\mathbf{e}[k] = \mathbf{x}[k] - \hat{\mathbf{x}}[k] \tag{9}$$

where $\hat{\mathbf{x}}[k]$ is the estimate state vector. The main objective of the KF algorithm is to minimise the error covariance matrix $\mathbf{P} \in \mathbb{R}^{N\times N}$ defined by,

$$\mathbf{P}[k] = E\{\mathbf{e}[k] \times \mathbf{e}[k]^{\mathbf{T}}\} \tag{10}$$

where E is the expected value operator. The *a priori* error covariance

matrix $\tilde{\mathbf{P}} \in \mathbb{R}^{N\times N}$ is defined as,

$$\tilde{\mathbf{P}}\ [k+1] = \mathbf{\Phi P}[k]\mathbf{\Phi}^{\mathbf{T}} + \mathbf{Q} \tag{11}$$

where $\mathbf{Q} \in \mathbb{R}^{N\times N}$ is the plant covariance error matrix associated to $\mathbf{w}$. The state variables vector $\tilde{\mathbf{x}}[k+1]$, *a priori* projected, are determined by (4). The estimate state vector $\hat{\mathbf{x}}[k+1]$ is updated using the Kalman filter gain as,

$$\mathbf{K}[k+1] = \tilde{\mathbf{P}}[k+1]\mathbf{H}^{\mathbf{T}}(\mathbf{H}\tilde{\mathbf{P}}\ [k+1]\mathbf{H}^{\mathbf{T}} + \mathbf{R})^{-1} \tag{12}$$

$$\hat{\mathbf{x}}[k+1] = \tilde{\mathbf{x}}[k+1] + \mathbf{K}[k+1](\mathbf{z}[k+1] - \mathbf{H}\tilde{\mathbf{x}}[k+1]) \tag{13}$$

where $\mathbf{R} \in \mathbb{R}^{N\times M}$ is the measurement error covariance matrix associated to the noise vector $\mathbf{v}$.

It is assumed that $\mathbf{Q}$ and $\mathbf{R}$ are uncorrelated and their mean values are zero. The state variables and the error covariance matrix in the first step are defined based on the initial condition, i.e. $\mathbf{x}_0$ and $\mathbf{P}_0$. The error covariance matrix is updated as,

$$\mathbf{P}[k+1] = (\mathbf{I} - \mathbf{K}[k+1]\mathbf{H})\tilde{\mathbf{P}}\ [k+1] \tag{14}$$

The iterative KF is executed during a time interval defined for each case study.

2.3. Half-wave symmetry

In this methodology, it is assumed that the power system is operating in periodic steady-state. Hence, distorted voltage and current waveforms are periodic. Symmetry of waveforms with respect to the origin of coordinates is called half-wave symmetry [27]. A periodic waveform $\boldsymbol{v}(t)$ is half-wave symmetrical if it satisfies

$$v(t) = -v\left(t \pm \frac{1}{2}T\right) \quad \forall\ t \tag{15}$$

Once the initial steady-state is determined, the KF is executed to determine the estimated voltage and current waveforms at unmonitored busbars. By exploiting the half-wave symmetry property, the KF is executed only a half-cycle [12,16]. If a cycle is divided into N samples, it is necessary to numerically process only $N/2$ samples.

Define $\hat{\mathbf{x}}_{\text{half}}$ as the estimated half-cycle. A full cycle can be formed using,

$$\hat{\mathbf{x}} = \hat{\mathbf{x}}_{\text{half}} \cup -\hat{\mathbf{x}}_{\text{half}} \tag{16}$$

where $\cup$ is the union operator.

2.4. Measuring process

The number and corresponding location of measuring devices are challenging tasks. Reference [28] reports a method in the time-domain to optimise the number of measuring devices and their respective locations.

Nowadays, the advanced metering infrastructure (AMI) is being implemented in power systems, which has led to the concept of smart grids. This enables access to voltage and current waveforms synchronized by global positioning system (GPS). Hence, the available data can be changed into useful information for the state estimation process.

State variables are the busbar voltages and the inductor branch currents; the measurements can be busbar voltages and inductor branch currents. [11,12]. Although busbar voltages correspond effectively to voltage measurements, the inductor branch currents in transmission lines, modelled by an equivalent π-model and the linear load, modelled by a RL parallel circuit, are not physically available. Reference [28] reports a procedure to incorporate to (8) the measurements corresponding to sending and receiving end line currents as well as RL parallel load currents.

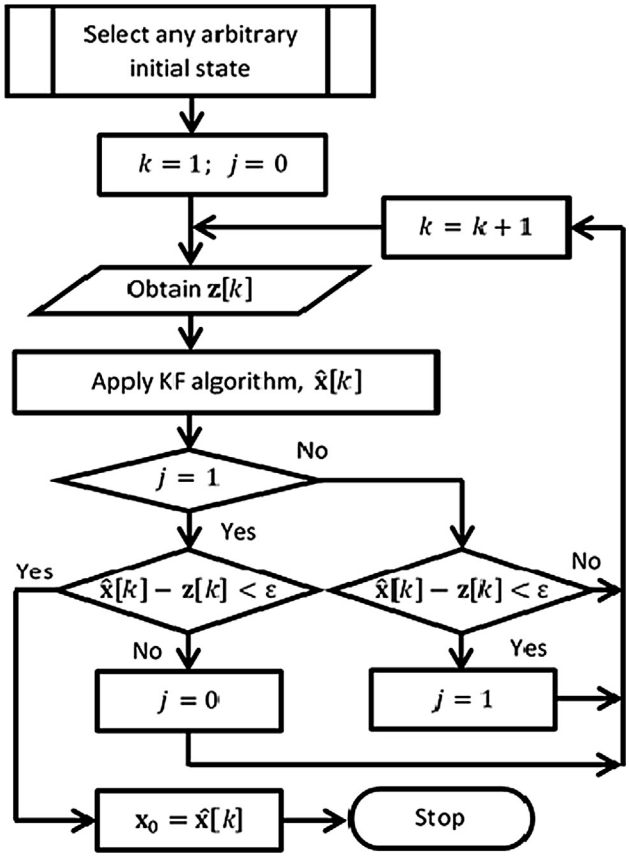

Fig. 2. Algorithm to obtain the periodic steady-state solution to synchronise measurements with the network model.

2.5. Periodic steady-state solution

As KF algorithm is based on an ODE discrete set; it needs an initial steady-state solution to begin the estimation process. In addition, as the KF algorithm takes the actual measurements to correct the prediction, they need to be synchronised with the plant model. In practical electrical grids, the measurements are taken from the network at any time; so they are not synchronized to the grid model defined in (8). Hence, a synchronised periodic steady-state solution to the measurements is needed [11,12].

In this research work, an alternative method to account for the periodic steady-state by the TDHSE algorithm is proposed. As it can be observed from Fig. 1, the method to determine the periodic steady-state solution uses the available measurements. The proposed algorithm is illustrated by the flowchart in Fig. 2 to achieve this solution. The description of the algorithm is detailed next.

First, the initial condition is defined. An arbitrary initial solution is proposed. It is common to set the initial state to zero. Two counters are defined: the k counter, defined previously as the sample number and a new counter named j that defines the number of times the sample is synchronised with the corresponding measurement. These counters are initially set to $k = 1$ and $j = 0$.

The KF algorithm is executed until the counter j reaches a sufficient number of times to ensure that synchronisation has been reached. To do that, the KF uses the initial solution and the available measurements taken from the physical electrical grid to perform an initial estimation, $\hat{\mathbf{x}}[k]$. This estimation is compared with the corresponding measurement vector $\mathbf{z}[k]$. If the comparison is less than a small number ε, it can be assumed that the actual sample is synchronised with the corresponding measurement and the counter j is increased. Otherwise, it is set to zero and the process continues for the next sample. If the counter j is

increased, a subsequent testing is done to ensure that the synchronisation is reached, i.e. two times is enough to consider that the periodic steady-state is achieved.

2.6. Fast fourier transform

The evaluation of the harmonic components in a distorted waveform is a challenging task [29–32]. If the electrical grid is considered in a steady-state, the FFT is used to determine the harmonic components in a distorted waveform, since it can perform fast conversion from time-domain to frequency domain [33]. These harmonic components are sinusoidal waveforms with frequency multiples of the fundamental frequency; each harmonic component has its own amplitude and phase. In this study, the FFT is applied to (16) to transform the time-domain data solution into the frequency domain response. The FFT allows the assessment of the total harmonic distortion (THD) of voltage and current waveforms. The power and demand factors can be obtained with these data under non-sinusoidal or harmonic distortion condition.

Prony's method is an alternative procedure to determine the harmonic spectrum from a signal, when dealing with short-time windows. However, the computational effort can be significant during the root-finding process of the polynomial equation used by the method. In addition, Prony's method is sensitive to noise, requiring an increase in the order of the model when noise is present in the resulting waveforms [34–37].

3. Experimental test electrical grid

3.1. Three-phase five-busbars test power system

Theoretical test systems have been proposed for harmonic analysis [38–40]. An experimental single-phase system, i.e. under balanced conditions, has been reported in [13]. For unbalanced condition, it is necessary to represent the plant as a three-phase circuit. The self and mutual parameters are needed.

In this contribution, an unbalanced three-phase five-busbar test electrical grid has been proposed for experimental HSE assessment and validation of the proposed TDHSE methodology. Fig. 3 shows the details of the actual laboratory implementation, including the location of three-phase voltage and current measurements. Please notice that the monitored locations are associated with busbars 1, 2 and 5; the unmonitored busbars are 3 and 4.

Different measurement configurations can be implemented. If the number of measurements is augmented, e.g., measuring voltages or currents at busbars 3 or 4, as more measurements are available to assess the state estimation, the estimation error has a tendency to decrease. If the number of measurements is decreased, e.g., due to instrument failure, bad calibration or communication link faults, the estimation error tends to increase, and some state variables are difficult to estimate, mainly those related to the lost measurements.

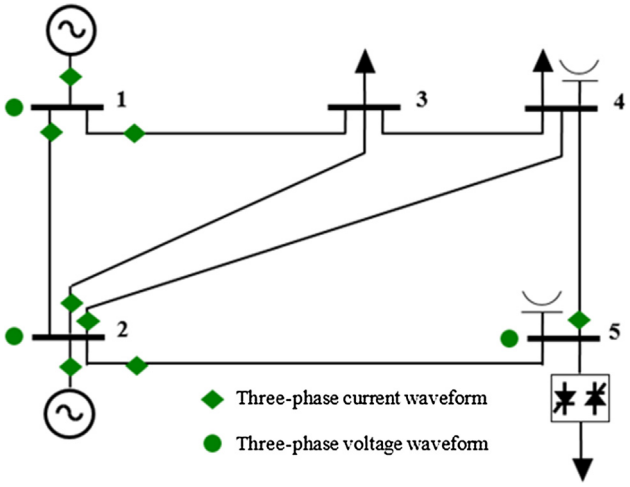

Fig. 3. Laboratory implementation of the proposed three-phase five-busbar test power system.

3.2. Three-phase power system modelling

3.2.1. Three-phase line model.

The three-phase lines are modelled by an equivalent π-circuit [41]. If symmetrical components are known, the line impedance matrix **Z** is given as,

$$\mathbf{Z} = \begin{bmatrix} \mathbf{Z}_{\text{self}} & \mathbf{Z}_{\text{mutual}} & \mathbf{Z}_{\text{mutual}} \\ \mathbf{Z}_{\text{mutual}} & \mathbf{Z}_{\text{self}} & \mathbf{Z}_{\text{mutual}} \\ \mathbf{Z}_{\text{mutual}} & \mathbf{Z}_{\text{mutual}} & \mathbf{Z}_{\text{self}} \end{bmatrix} \tag{17}$$

where $\boldsymbol{Z}_{\text{self}} = (2\boldsymbol{Z}^{+\text{Seq}} + \boldsymbol{Z}^{0\text{Seq}})/3$ and $\boldsymbol{Z}_{\text{mutual}} = (\boldsymbol{Z}^{0\text{Seq}} - \boldsymbol{Z}^{+\text{Seq}})/3$. The KF can consider insufficient knowledge of parameters. For the experimental test system, the mutual impedance is set to zero. Hence, the matrix **Z** is given by,

$$\boldsymbol{Z} = \begin{bmatrix} \boldsymbol{Z}_{\text{self}} & 0 & 0 \\ 0 & \boldsymbol{Z}_{\text{self}} & 0 \\ 0 & 0 & \boldsymbol{Z}_{\text{self}} \end{bmatrix} \tag{18}$$

3.2.2. Three-phase generator model.

Synchronous generators can be modelled in several ways [42,43]. For the case study to be reported, the units are represented by a sinusoidal voltage source behind an impedance. The mutual impedance is assumed to be zero. Hence, the generator impedance $\mathbf{Z}_{\mathbf{G}}$ is given as,

$$\mathbf{Z}_{\mathbf{G}} = \begin{bmatrix} \boldsymbol{R}_a + \boldsymbol{L}_{\text{self}} & 0 & 0 \\ 0 & \boldsymbol{R}_a + \boldsymbol{L}_{\text{self}} & 0 \\ 0 & 0 & \boldsymbol{R}_a + \boldsymbol{L}_{\text{self}} \end{bmatrix} \tag{19}$$

3.2.3. Three-phase linear load model.

The three-phase linear loads are modelled as RL branches. Hence, the impedance of the linear load is given by,

$$\mathbf{Z}_{\mathbf{L}} = \begin{bmatrix} \boldsymbol{R}_{\text{load}} + \boldsymbol{L}_{\text{load}} & 0 & 0 \\ 0 & \boldsymbol{R}_{\text{load}} + \boldsymbol{L}_{\text{load}} & 0 \\ 0 & 0 & \boldsymbol{R}_{\text{load}} + \boldsymbol{L}_{\text{load}} \end{bmatrix} \tag{20}$$

3.2.4. Three-phase nonlinear load model.

The three-phase nonlinear load is modelled as injected harmonic current sources [44,45], i.e.,

$$\mathbf{I}_{\mathbf{H}} = \begin{bmatrix} \boldsymbol{I}_1\angle 0 + \boldsymbol{I}_2\angle 0 + \cdots + \boldsymbol{I}_h\angle 0 \\ \boldsymbol{I}_1\angle 120 + \boldsymbol{I}_2\angle 120 + \cdots + \boldsymbol{I}_h\angle 120 \\ \boldsymbol{I}_1\angle -120 + \boldsymbol{I}_2\angle -120 + \cdots + \boldsymbol{I}_h\angle -120 \end{bmatrix} \tag{21}$$

3.3. Implementation of the three-phase five-busbar electrical power grid

The experimental three-phase five busbar electrical grid has been implemented in laboratory using the Electromechanical Training Systems model 8013 of Lab-Volt [46]. The modules consist of synchronous generators, medium-length transmission lines, capacitor banks and electrical linear loads. The line to line base voltage and the three-phase base apparent power are 208 V and 900VA, respectively. Fig. 4 shows the wiring test power system.

The self-parameters for lines, generators, linear loads, and injected vars are given in Tables 1–4, respectively.

The nonlinear load is represented by the injected harmonics at busbar 5 in phases A and C. There is no harmonic current injection in phase B to increase the unbalanced condition of the test system. The

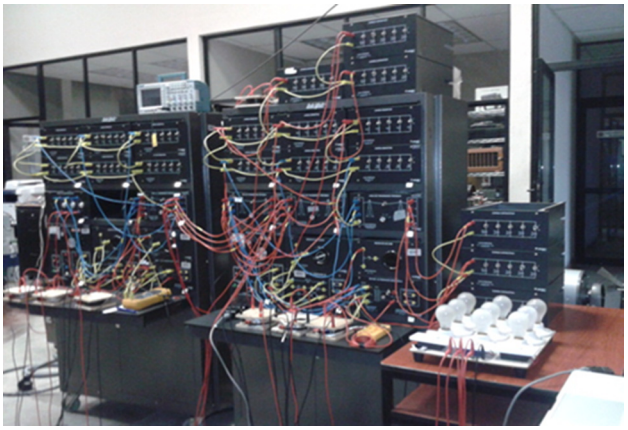

Fig. 4. Wired three-phase five-busbar test electrical power grid.

Table 1
Self parameters of transmission lines.

Lines	Impedance	Line charging
1–2	0.02 + j0.06	j0.030
1–3	0.08 + j0.27	j0.025
2–3	0.06 + j0.18	j0.020
2–4	0.06 + j0.18	j0.020
2–5	0.04 + j0.12	j0.010
3–4	0.01 + j0.03	j0.010
4–5	0.08 + j0.27	j0.025

Table 2
Self parameters of synchronous generators.

Generator	Impedance
1	0.0125 + j0.3848
2	0.125 + j0.3848

Table 3
Self parameters of linear electrical loads.

Busbar	Watts	Vars
1	0	0
2	0	0
3	0.4	0.2
4	0.8	0.4
5	0.6	0

Table 4
Self parameters of injected vars.

Busbar	Vars
4	0.4
5	0.2

unbalanced three-phase harmonic source is generated by an incandescent light dimmer per phase connected at busbar 5, as detailed next.

Fig. 5 shows the three-phase unbalanced nonlinear load. It consists of parallel incandescent lights with a control circuit consisting of a dimmer bridge based on silicon-controlled rectifiers. The thyristor firing angle can be adjusted to control the load power flow. Each dimmer has been set to a different value to obtain an unbalanced three-phase nonlinear load. These nonlinear loads inject a wide range of harmonic components into the power system [29]. The unbalanced harmonics injected at busbar 5 are given in Table 5.

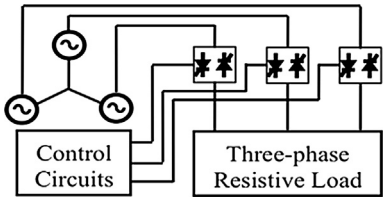

Fig. 5. Thyristor-controlled three-phase resistive circuit modelling a nonlinear load connected to busbar 5.

Table 5
Unbalanced harmonics injected at busbar 5.

Order	% Phase A fundamental	Phase A (rad)	% Phase C fundamental	Phase C (rad)
3	15.0225	0.2573	52.4612	−1.2070
5	13.5759	−1.9159	20.3254	−1.0810
7	4.2622	2.2053	10.1592	−0.9570
9	5.1704	0.6350	11.8031	0.2477
11	4.5197	−2.2071	13.1627	0.0228

3.4. Measurement process implementation

The data acquisition system has been implemented with the Tektronix TDS2024C, 200 MHz, 4 Channels, and 2 GS/s Digital Storage Oscilloscope, which can be connected to a computer using the rear-panel USB device port for data transfer. Passive voltage electrodes provide a low cost, general purpose voltage testing solution. However, for current measurement, current probes were used to enable the oscilloscope to measure current, extending its use beyond just measuring voltage. As measurements need to be synchronised, a common channel was used to ensure this condition.

3.5. Detailed modelling of three-phase five busbars test system

Since the system has 7 transmission lines, 2 linear loads, 2 generators and 5 busbars, $16 \times 3 = 48$ state variables are defined. Hence, according to (4) and using linear algebra and circuit theory, the test system model is represented by a set of 48 first-order ODE's. Table 6 indicates the selected state variables and their corresponding names.

The state variables in the first five rows of Table 6 indicate the phase voltage of busbars 1–5, phases A, B, and C. The following two rows indicate the phase current of generators 1 and 2, phases A, B, and C, respectively; rows 8–14 indicate state variables for phase current in lines, phases A, B, and C. The last two rows indicate the state variables for the load inductive current of busbars 3 and 4, phases A, B, and C,

Table 6
Three-phase state variables and physical variables.

State variable	Physical variable
$x1$, $x17$, $x33$	Phase voltages, busbar 1
$x2$, $x18$, $x34$	Phase voltages, busbar 2
$x3$, $x19$, $x35$	Phase voltages, busbar 3
$x4$, $x20$, $x36$	Phase voltages, busbar 4
$x5$, $x21$, $x37$	Phase voltages, busbar 5
$x6$, $x22$, $x38$	Phase currents, generator 1
$x7$, $x23$, $x39$	Phase currents, generator 2
$x8$, $x24$, $x40$	Phase currents, line 1–3
$x9$, $x25$, $x41$	Phase currents, line 1–2
$x10$, $x26$, $x42$	Phase currents, line 2–3
$x11$, $x27$, $x43$	Phase currents, line 2–4
$x12$, $x28$, $x44$	Phase currents, line 2–5
$x13$, $x29$, $x45$	Phase currents, line 3–4
$x14$, $x30$, $x46$	Phase currents, line 4–5
$x15$, $x31$, $x47$	Load inductive currents, busbar 3
$x16$, $x32$, $x48$	Load inductive currents, busbar 4

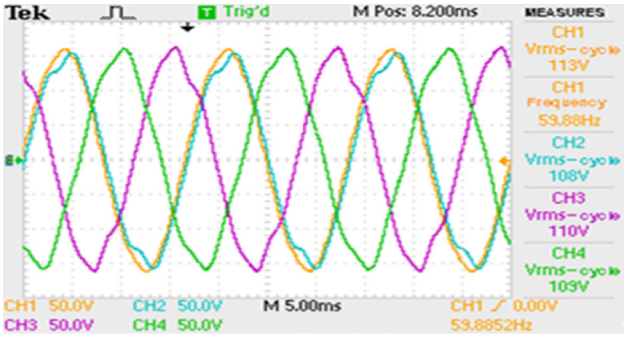

Fig. 6. The oscilloscope waveforms of the three-phase voltage at busbar 3.

respectively. The variables $\boldsymbol{x}$1-16 represent the phase A state variables. The state variables $\boldsymbol{x}$1 to $\boldsymbol{x}$5 represent the busbar voltages 1–5, $\boldsymbol{x}$6 and $\boldsymbol{x}$7 represent the generator currents 1–2, $\boldsymbol{x}$8 to $\boldsymbol{x14}$ represent the lines currents, and x15-16 the load inductive currents. Similarly, state variables $\boldsymbol{x}$17-32 correspond to phase B, and state variables $\boldsymbol{x}$33-48 to phase C.

4. Results

4.1. Test system based harmonic state

The actual harmonic state is obtained from the test system set up shown in Fig. 3. Measurements have been taken with the digital oscilloscope, set to $Fs = 50{,}000$ samples per second. These practical measurements define the actual harmonic state. The busbar voltages, sending, and receiving end line currents have been recorded. Fig. 6 shows the three-phase voltages at busbar 3, displayed by the oscilloscope. An average of 1.8% of unbalance between phases can be observed. The unbalanced harmonic condition is given in Table 5. The phase A voltage at busbar 1 has been taken as a reference and continuously measured in channel 1 to synchronize the rest of the measurements; channels 2 to 4 measure phases A (channel 2), B (channel 4), and C (channel 3), respectively. Although there are no injected harmonics in phase B, it may be observed that the waveform of phase B contains harmonic distortion due to electromagnetic coupling. In addition, there is a phase shift between busbars 1 and 3.

4.2. Periodic steady-state solution

The measuring devices placed as shown in Fig. 3 provide measurements of busbar voltages and of sending and receiving line currents that have been incorporated into the measurement equation. Hence, the resulting measurement vector is $\mathbf{z} \in \mathbb{R}^{33}$ and since $\mathbf{x} \in \mathbb{R}^{48}$, the resulting measurement matrix is $\mathbf{H} \in \mathbb{R}^{33\times48}$.

The harmonic state estimation solution has been obtained with the proposed method and compared against the response obtained with the previously-developed methodologies [11,12,20]. The trajectory of the three-phase voltage at unmonitored busbar 3 is analysed. The particular solution found will be indicated with black circles in the corresponding figures.

The EMTDC® based on the trapezoidal rule (TR), has been used to determine the periodic steady-state solution. This method is also known as Brute Force (BF) method due to the long-time taken to reach the steady-state. The particular solution is reached in the cycle 45, i.e. 750 ms. Fig. 7 shows the trajectory response to reach this solution. Only the first and last two cycles are shown with more detail.

Fig. 8 shows the response to reach the steady-state solution by the Numerical Differentiation (ND) method. The steady-state solution is reached after 4 cycles, i.e. 66.66 ms. ND takes the first-order ODE set which models the system and evaluates the periodic steady-state using the Poincaré map and the limit cycle extrapolation of the state variables

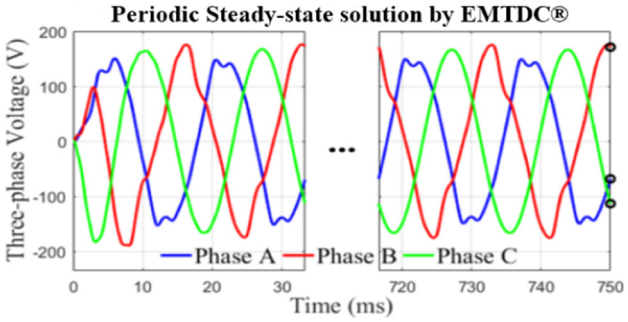

Fig. 7. Periodic steady-state solution is obtained using EMTDC® for the three-phase voltage of unmonitored busbar 3.

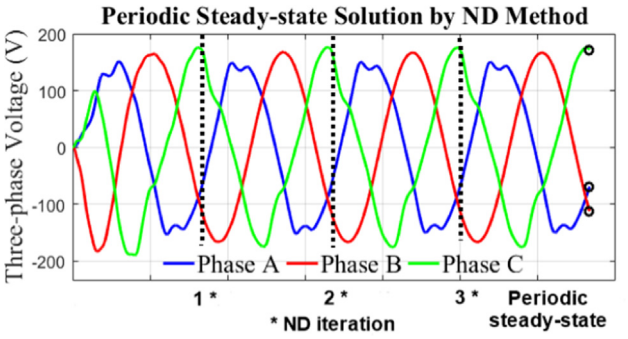

Fig. 8. Unbalanced three-phase voltage at unmonitored busbar 3, ND periodic steady-state after 3 iterations or 66.6 ms.

[11]. Firstly a base cycle is obtained and with a perturbed value at the base cycle beginning the difference between the last two values is used to obtain the state variable difference, which allows to identify the state transition matrix, in turn this matrix is used to calculate the limit cycle for the state variables [20].

Fig. 9 shows the periodic steady-state solution obtained with the Enhanced Numerical Differentiation (END) method [12]. The time to determine this solution has been only 3 cycles, i.e. 50 ms. These solutions need to be synchronised with the electrical grid model and the measurements taken from the physical electrical grid.

Now, the steady-state solution is obtained by applying the proposed algorithm shown in Fig. 2. Different initial states have been used to evaluate the performance of the proposed algorithm. Fig. 10 shows the time-domain evolution to find the three-phase voltage steady-state solution using different arbitrary initial states at the unmonitored busbar 3. The steady-state solution is reached at sample 335, i.e. in 6.7 ms. This reduced time is due to the method is taking into account the available measurements. As the method uses the measurements from the physical electrical grid, the solution is synchronised with it. The comparison of results between the proposed algorithm and previous ones, i.e. the

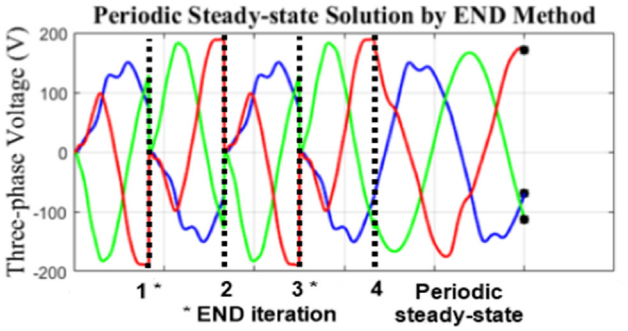

Fig. 9. Periodic steady-state solution is obtained using the END method after 4 iterations or 50 ms.

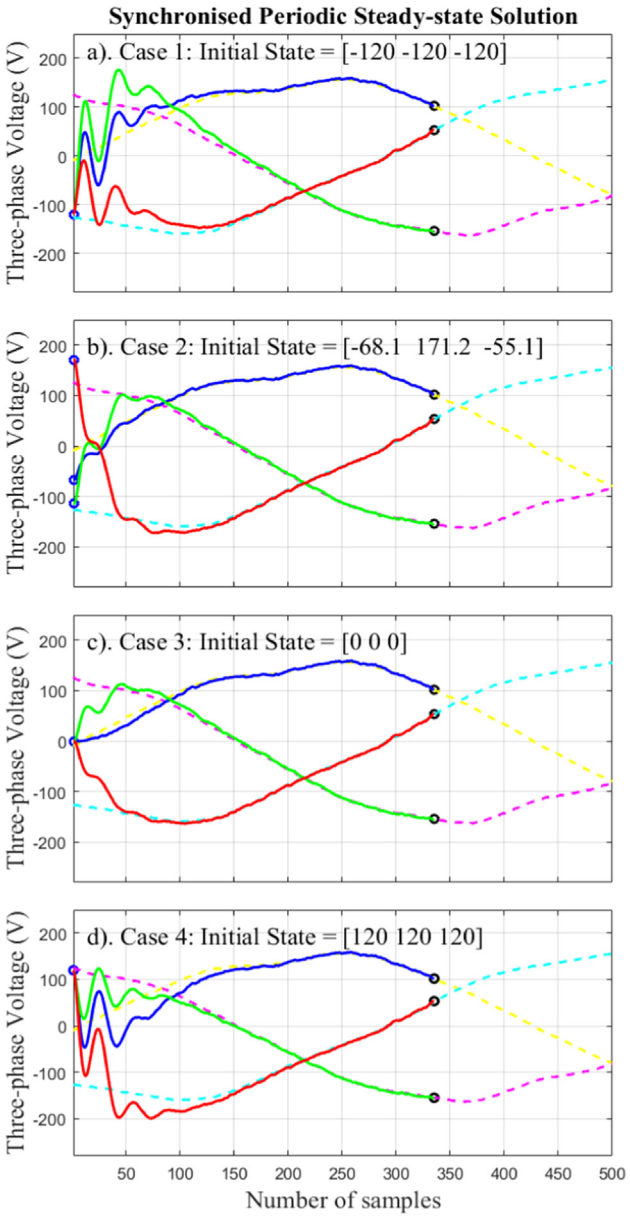

Fig. 10. Periodic steady-state solution is obtained using an arbitrary initial state of a) −120 V, b) −68.1 V, c) 0 V, and d) 120 V.

Table 7
Execution time and synchronization.

Parameter	EMTDC® [19]	ND [11]	END [12]	Proposed method
Time (ms) to reach the steady-state	750	66.66	50	15
Synchronized with the electrical grid	No	No	No	Yes

EMTDC® using the TR [19] and the methods reported in [11–12], are highlighted in Table 7. It is relevant to mention that the proposed method is 3.3, 4.4 and 50 times faster than the one reported in [12,11], and [19], respectively.

The reduced time of the proposed method is due to the use of available measurements and the numerical process based on the KF to determine first the steady-state and then the state estimation. It lasts 6.7 ms to reach the sample 335 (Fig. 10) plus half-cycle or 8.3 ms to apply the KF to assess the state estimation completing 15 ms. EMTDC®, ND, and END methods do not use measurements, they are based on numerical methods.

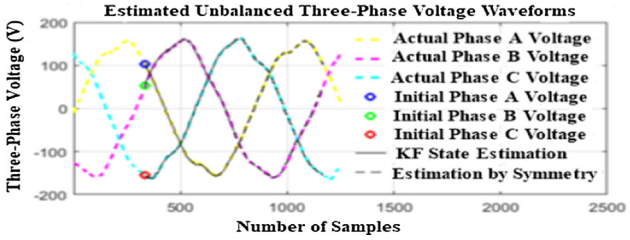

Fig. 11. Actual (laboratory) and estimated unbalanced three-phase voltage at the unmonitored busbar 3.

4.3. Time-domain harmonic state estimation

Once the steady-state solution is found, the estimation of voltage and current can be performed. For illustrative purposes, the unbalanced three-phase voltage waveform at unmonitored voltage busbar 3 is analysed. The particular steady-state solution commences at time t = 750 ms being 102.19, 53.56, and −154.61 Volts for phases A, B, and C, respectively. It has been marked with circles in Figs. 10 and 11. The actual three-phase voltage waveforms are also shown in Fig. 11. These waveforms have been taken from the test power grid implemented in laboratory. It can be observed that the solution is synchronised with the physical electrical grid. Now, with the execution of the KF algorithm during a half-cycle, half-cycle voltage waveform is estimated. These estimated waveforms are shown in Fig. 11 in continuous black line. By exploiting the half-wave symmetry property, a full-cycle of the voltage waveforms is estimated. They are shown in Fig. 11 with the discontinuous black line. Hence, the unbalanced three-phase voltage waveforms at the unmonitored busbar 3 has been accurately estimated. It can be observed that despite the insufficient knowledge of the plant model parameters, the estimation is in close agreement with the actual voltage waveforms.

4.4. Total harmonic distortion assessment

Once the voltage and current waveforms have been estimated, the FFT algorithm is applied to obtain the THD for voltages (although THD for currents can be also obtained). Table 8 gives the THD as a percentage of the fundamental component for phase voltages at unmonitored busbar 3. It can be observed that the estimated THD agrees well with the actual harmonic spectra obtained from recorded data. The maximum absolute difference between the actual laboratory THD and the THD obtained with the proposed methodology is 0.29% for phase A and the average error is 0.18%. For these unbalanced operating conditions, a THD of 5.78% was estimated in phase B using the proposed methodology.

The minimum and maximum absolute errors are determined by comparing the absolute error of the three phases. The average and the standard deviation are evaluated by using the 3A, 3B, and 3C phase values of the laboratory test and KF estimation columns of Table 8. The

Table 8
Phase voltage thd (%) at unmonitored busbar 3.

Phase	Laboratory test	KF estimation	Absolute error
3A	5.9204	5.6234	0.2970
3B	5.8999	5.7868	0.1131
3C	5.1117	4.9745	0.1372
Minimum absolute error (3B)	5.8999	5.7868	0.1131
Maximum absolute error (3A)	5.9204	5.6234	0.2970
Average	5.6440	5.4615	0.1825
Standard deviation	0.3764	0.3508	0.0256

absolute error is the difference between the laboratory test and the KF estimation values. The THD is below 5.93% for all values including the average value; these THD values are due to the unbalanced nonlinear load connected at busbar 5. The standard deviation is also below 0.38%, and the absolute error is below 0.3% for all values, which shows the good agreement achieved between the laboratory test and the KF state estimation.

5. Conclusions

An enhanced time-domain methodology to determine the harmonic state estimation for unbalanced three-phase electrical power grids has been proposed. The methodology allows synchronization between the limited number of measurements taken from the physical electrical grid and its mathematical modelling. This algorithm has been synchronously applied to determine the periodic steady-state solution for an electrical grid using the available limited number of measurements and the Kalman filter.

The proposed TDHSE method is 3.3, 4.4, and 50 times faster than the END, ND, and the time-domain solution using EMTDC®, respectively, since the TDHSE uses a half cycle instead of one cycle, to obtain the harmonic state solution due to the half-wave symmetry property in the voltage and current waveforms, and also uses measurements associated with the KF to obtain the steady-state and the state estimation result.

The results have been successfully tested and validated against experimental data instead of synthetic data. The proposed TDHSE methodology has been validated through direct comparison of the estimated (unmonitored) state variables against the corresponding physical variables directly measured from the laboratory experiment. A close agreement between simulated and experimental responses has been obtained in all cases.

Credit authorship contribution statement

Ismael Molina-Moreno: Conceptualization, Formal analysis, Investigation, Methodology, Software, Validation, Visualization, Writing - original draft, Writing - review & editing. **Aurelio Medina:** Conceptualization, Formal analysis, Funding acquisition, Methodology, Project administration, Resources, Supervision, Visualization, Writing - original draft, Writing - review & editing. **Rafael Cisneros-Magaña:** Conceptualization, Formal analysis, Investigation, Methodology, Software, Validation, Visualization, Writing - original draft, Writing - review & editing. **Olimpo Anaya-Lara:** Visualization, Writing - original draft, Writing - review & editing. **Juan Alfonso Salazar-Torres:** Visualization, Writing - original draft, Writing - review & editing.

Declaration of Competing Interest

The authors declare that they have no known competing financial interests or personal relationships that could have appeared to influence the work reported in this paper.

Acknowledgements

The authors gratefully acknowledge the facilities granted to carry out this investigation by Universidad Michoacana de San Nicolas de Hidalgo, Facultad de Ingeniería Eléctrica, División de Estudios de Posgrado (FIE-DEP) Morelia, México. The authors thank the financial aid received from CONACYT for this research work.

References

[1] Dugan RC, McGranaghan MF, Santoso S, Beaty HW. Electrical Power Systems Quality. McGraw-Hill Education: Third Edition; 2012.
[2] Saini MK, Kapoor R. Classification of power quality events - A review. Int. J. Electr. Power Energy Syst. 2012;43(1):11–9.
[3] Sazli MH, Koşalay İ, Erdenesaikhan G. A brief review of power quality issues in smart grid and a simple user friendly software. 2018 6th International Istanbul Smart Grids and Cities Congress and Fair (ICSG). 2018. p. 54–8.
[4] Arrillaga J, Watson NR, Chen S. Power system quality assessment. John Wiley & Sons; 2000.
[5] Farzanehrafat A, Watson NR. Power Quality State Estimator for Smart Distribution Grids. IEEE Trans. Power Syst. 2013;28(3):2183–91.
[6] Cisneros-Magaña R, Medina A, Dinavahi V, Ramos-Paz A. Time-Domain Power Quality State Estimation Based on Kalman Filter Using Parallel Computing on Graphics Processing Units. IEEE Access 2018;6:21152–63.
[7] Achlerkar PD, Samantaray SR, Manikandan MS. Variational Mode Decomposition and Decision Tree Based Detection and Classification of Power Quality Disturbances in Grid-Connected Distributed Generation System. IEEE Trans. Smart Grid 2018;9(4):3122–32.
[8] Rakpenthai C, Uatrongjit S, Watson NR, Premrudeepreechacharn S. On Harmonic State Estimation of Power System With Uncertain Network Parameters. IEEE Trans. Power Syst. 2013;28(4):4829–38.
[9] Almeida CFM, Kagan N. Harmonic state estimation through optimal monitoring systems. IEEE Trans. Smart Grid 2013;4(1):467–78.
[10] Moradifar A, Foroud AA, Firouzjah KG. Intelligent localisation of multiple nonlinear loads considering impact of harmonic state estimation accuracy. IET Gener. Transm. Distrib. 2017;11:1943–53.
[11] Medina A, Cisneros-Magana R. Time-domain harmonic state estimation based on the kalman filter poincare map and extrapolation to the limit cycle. IET Gener. Transm. Distrib. 2012;6(12):1209–17.
[12] Cisneros-Magaña R, Medina A, Segundo-Ramírez J. Efficient time domain power quality state estimation using the enhanced numerical differentiation Newton type method. Int. J. Electr. Power Energy Syst. 2014;63:414–22.
[13] Molina-Moreno I, Medina A, Cisneros-Magana R. "Experimental time domain harmonic state estimation using partial measurements", *2014 North Am.* Power Symp. NAPS 2014;2014:1–6.
[14] Molina-Moreno I, Medina A, Cisneros-Magaña R. Time-domain harmonic state estimation using filtered measurements based on Fourier transform. North American Power Symposium (NAPS) 2015;2015:1–6.
[15] Molina-Moreno I, Medina A, Cisneros-Magaña R, Anaya-Lara O. Time domain harmonic state estimation in unbalanced power networks based on optimal number of meters and the principle of half-wave symmetry. IET Gener. Transm. Distrib. 2017;11(15):3871–80.
[16] I. Molina-Moreno, A. Medina, R. Cisneros-Magaña, and O. Anaya-Lara, "Noise mitigation in voltage and current waveforms in harmonic distortion estimation," in 2017 IEEE International Autumn Meeting on Power, Electronics and Computing (ROPEC), 2017, pp. 1–6.
[17] Watson NR. Power quality state estimation. Eur. Trans. Electr. Power Jan. 2010;20(1):19–33.
[18] N. Watson, J. Arrillaga, and I. of E. Engineers, Power Systems Electromagnetic Transients Simulation. Institution of Engineering and Technology, 2003.
[19] Manitoba HVDC Research Centre, "EMTDC Transient Analysis for PSCAD Power System Simulation: Users's Guide," pp. 1–233, 2010.
[20] Semlyen A, Medina A. Computation of the periodic steady state in systems with nonlinear components using a hybrid time and frequency domain methodology. IEEE Trans. Power Syst. 1995;10(3):1498–504.
[21] Díaz-Araujo MH, Medina-Rios JA. Periodic steady state of power networks using the numerical differentiation method and spline interpolation. IEEE Power Energy Soc. General Meeting 2017;2017:1–5.
[22] K. Ogata, Discrete-time Control Systems. Prentice-Hall International, 1995.
[23] Beides HM, Heydt GT. Dynamic state estimation of power system harmonics using Kalman filter methodology. Power Deliv. IEEE Trans. 1991;6(4):1663–70.
[24] Grewal MS, Andrews AP. Kalman Filtering: Theory and Practice with MATLAB. Wiley; 2015.
[25] Bagheri A, Mardaneh M, Rajaei A, Rahideh A. Detection of Grid Voltage Fundamental and Harmonic Components Using Kalman Filter and Generalized Averaging Method. IEEE Trans. Power Electron. 2016;31(2):1064–73.
[26] Qi J, Sun K, Wang J, Liu H. Dynamic State Estimation for Multi-Machine Power System by Unscented Kalman Filter With Enhanced Numerical Stability. IEEE Trans. Smart Grid 2018;9(2):1184–96.
[27] Kumar KSS. Electric Circuits and Networks. Dorling Kindersley; 2009.
[28] Molina-Moreno I, Medina A, Cisneros-Magana R, Anaya-Lara O. A Methodology for Transient State Estimation Based on Numerical Derivatives, Optimal Monitoring, and Filtered Measurements. IEEE Trans. Power Deliv. 2018;33(4):1527–35.
[29] Arrillaga J, Smith BC, Watson NR, Wood AR. Power System Harmonic Analysis. Wiley; 1997.
[30] Wen H, Zhang J, Meng Z, Guo S, Li F, Yang Y. Harmonic Estimation Using Symmetrical Interpolation FFT Based on Triangular Self-Convolution Window. IEEE Trans. Ind. Informatics 2015;11(1):16–26.
[31] Enayati J, Moravej Z. Real-time harmonics estimation in power systems using a novel hybrid algorithm. IET Gener. Transm. Distrib. 2017;11(14):3532–8.
[32] Walker JS. Fast Fourier Transforms. CRC Press; 2017.
[33] Goh ZP, Radzi MAM, Von Thien Y, Hizam H, Abdul NI. Wahab, "Hybrid FFT-ADALINE algorithm with fast estimation of harmonics in power system", *IET*. Signal Process. 2016;10(8):855–64.
[34] Chen C, Chang GW. An Efficient Prony-Based Solution Procedure for Tracking of Power System Voltage Variations. IEEE Trans. Ind. Electron. 2013;60(7):2681–8.
[35] S. Føyen, M. Kvammen, and O. B. Fosso, "Prony's method as a tool for power system identification in Smart Grids," in 2018 International Symposium on Power Electronics, Electrical Drives, Automation and Motion (SPEEDAM), 2018, pp.

562–569.
[36] Akke M. Frequency estimation by demodulation of two complex signals. IEEE Trans. Power Deliv. 1997;12(1):157–63.
[37] T. Hasan, "Complex demodulation: Some theory and applications," in Time Series in the Frequency Domain, vol. 3, Elsevier, 1983, pp. 125–156.
[38] Bonner A, et al. Modeling and simulation of the propagation of harmonics in electric power networks. Part II: sample systems and examples. IEEE Trans. Power Deliv. 1996;11(1):466–72.
[39] Task Force on Harmonics Modeling and Simulation, "Modeling and simulation of the propagation of harmonics in electric power networks. I. Concepts, models, and simulation techniques," IEEE Trans. Power Deliv., 11 (1), pp. 452–465, 1996.
[40] Acha E, Madrigal M. Power Systems Harmonics: Computer Modelling and Analysis. Wiley; 2001.
[41] Grainger JJ, Stevenson WD, Chang GW. Power System Analysis. McGraw-Hill Education; 2016.
[42] Despalatovic M, Jadric M, Terzic B. Modeling of Saturated Synchronous Generator Based on Steady-State Operating Data. IEEE Trans. Ind. Appl. 2012;48(1):62–9.
[43] Garcia N, Acha E. Periodic steady-state solution of a synchronous generator based on a voltage-behind-reactance formulation and the Poincaré map method. Int. J. Electr. Power Energy Syst. 2013.
[44] S. Chreang and P. Kumhom, "A study of nonlinear DC and AC loads connected to PV microgrid," Proc. 2018 5th Int. Conf. Bus. Ind. Res. Smart Technol. Next Gener. Information, Eng. Bus. Soc. Sci. ICBIR 2018, pp. 309–313, 2018.
[45] L. Manuel, B. Josep, M. Juan, C. Montserrat, and G. Eulalia, "Modelling harmonics drawn by nonlinear loads," Proc. - 2015 9th Int. Conf. Compat. Power Electron. CPE 2015, pp. 93–97, 2015.
[46] Festo Didactic Inc, "2 kW Electromechanical Training Systems," 2015. [Online]. Available: https://www.labvolt.com/solutions/6_electricity_new_energy/98-8013-00_2_kw_electromechanical_training_systems.

Ismael Molina-Moreno was born in Morelia, México, on May 20, 1964. He received the B.Eng. and M.Sc. degrees from the Tecnológico Nacional de México, México, and the Ph.D. degree from the Universidad Michoacana de San Nicolás de Hidalgo, Mexico in 1988, 2004, and 2017, respectively. He joined Tecnológico Nacional de México/I.T. Morelia in 2004. His fields of interest include power quality state estimation and power electronics.

Aurelio Medina obtained his Ph.D. from the University of Canterbury, Christchurch, New Zealand in 1992. He has worked as a Post-Doctoral Fellow at the Universities of Canterbury, New Zealand (1 year) and Toronto, Canada (2 years). He joined the Facultad de Ingeniería Eléctrica, UMSNH, Morelia, México, in 1995. He is a Senior Member of the IEEE. His research interests are in the analysis of power quality phenomena, dynamic and steady-state analysis of power systems, renewable energy systems and application of advanced numerical and computer techniques to power system analysis.

Rafael Cisneros-Magaña received his M.Sc. and Ph.D. degrees in electrical engineering from the Faculty of Electrical Engineering, Universidad Michoacana de San Nicolás de Hidalgo, Morelia, Mexico in 2009 and 2013, respectively. He had a research stay in the University of Alberta, Edmonton, Canada in 2012 (1-year) to apply the numerical parallel processing to power systems. His current research interests are in modelling, analysis and simulation of power systems, time-domain state estimation, power quality adverse phenomena, renewable energy systems including wind and photovoltaic generation, power electronics and electromagnetic transients and numerical parallel processing applied to power system state estimation.

Olimpo Anaya-Lara received the B.Eng. and M.Sc. degrees from Instituto Tecnológico de Morelia, Morelia, México, and the Ph.D. degree from the University of Glasgow, Glasgow, U.K., in 1990, 1998, and 2003, respectively. His industrial experience includes periods with Nissan Mexicana, Toluca, México, and CSG Consultants, Coatzacoalcos, México. Currently, he is a Professor with the Institute for Energy and Environment, University of Strathclyde, Glasgow, U.K. His current research interests include wind generation, power electronics, and stability of mixed generation power systems.

Juan Alfonso Salazar-Torres was born in Toluca, Mexico, in 1979. He received the Ph.D. degree in electronic engineering from the Instituto Tecnológico de Toluca, Mexico, in 2014. He was involved in the development of power supply devices, induction furnace, electronic instrumentation, power electronics, control systems, modelling and simulation of process, plasma diagnostics, degradation of toxic gas and energy recovery. He is currently a professor-researcher of the National Council for Science and Technology CONACYT since 2014. He is a member of the Sistema Nacional de Investigadores in Mexico since 2015.